

Hurricane Forecasting: A Novel Multimodal Machine Learning Framework

LÉONARD BOUSSIOUX*

Operations Research Center, Massachusetts Institute of Technology, Cambridge, MA, USA
leobix@mit.edu

CYNTHIA ZENG*

Operations Research Center, Massachusetts Institute of Technology, Cambridge, MA, USA
czeng12@mit.edu

THÉO GUÉNAIS

School of Engineering and Applied Sciences, Harvard University, Cambridge, MA, USA
tguenais@fas.harvard.edu

DIMITRIS BERTSIMAS[†]

Sloan School of Management and Operations Research Center, Massachusetts Institute of Technology, Cambridge, MA, USA
dbertsim@mit.edu

ABSTRACT

This paper describes a machine learning (ML) framework for tropical cyclone intensity and track forecasting, combining multiple distinct ML techniques and utilizing diverse data sources. Our framework, which we refer to as Hurricast (HURR), is built upon the combination of distinct data processing techniques using gradient-boosted trees and novel encoder-decoder architectures, including CNN, GRU and Transformers components. We propose a deep-feature extractor methodology to mix spatial-temporal data with statistical data efficiently. Our multimodal framework unleashes the potential of making forecasts based on a wide range of data sources, including historical storm data, reanalysis atmospheric images, and operational forecasts. Evaluating our models with current operational forecasts in North Atlantic and Eastern Pacific basins on the last years of available data, results show our models consistently outperform statistical-dynamical models and, albeit less accurate than the best dynamical models, our framework computes forecasts in seconds. Furthermore, the inclusion of Hurricast into an operational forecast consensus model leads to a significant improvement of 5% - 15% over NHC's official forecast, thus highlighting the complementary properties with existing approaches. In summary, our work demonstrates that combining different data sources and distinct machine learning methodologies can lead to superior tropical cyclone forecasting.

Significance statement. A new machine learning framework for tropical cyclone track and intensity forecasting by combining multiple distinct methodologies to utilize diverse data sources. Evaluation results suggest our approach is competitive to operational forecasts, and can bring additional value to improve consensus models.

1. Introduction

A tropical cyclone (TC) is a rapidly rotating storm originating from the tropical ocean and developing by drawing energy from the sea. It is characterized by a low-pressure center, known as the "eye", a closed low-level atmospheric circulation, strong winds, and spiraling thunderstorms which relieve energy by producing heavy rain. Every year, tropical cyclones cause hundreds of deaths and

billions of dollars of damage to households and businesses (Grinsted et al. 2019). Moreover, there is growing evidence suggesting consistent hurricane intensity escalation due to climate change, leading to potentially greater damaging power (Knutson et al. 2019). Therefore, producing an accurate prediction for hurricane track and intensity with sufficient lead time is critical to undertake life-saving measures.

TC forecasting encompasses several tasks, including, in particular: track forecasting, i.e., the prediction of the hurricane trajectory; intensity forecasting, i.e., predicting intensity measures such as the maximum sustained wind speed in a particular time interval. Generally speaking, current operational TC forecasts can be classified into numerical models, statistical models and ensemble models (Rhome 2007). Numerical models, also known as dynamical models, utilize powerful supercomputers to simulate atmospheric fields' evolution using sophisticated

*Equal contribution

[†]Corresponding author: Dimitris Bertsimas, dbertsim@mit.edu

physically-motivated dynamical equations. Major operational numerical models include the Hurricane Weather and Research Forecasting model (HWRF), the Global Forecast System (GFS), and the European Center for Medium-Range Weather Forecasts (ECMWF) global model (EMX). On the other hand, statistical models approximate historical relationships between storm behavior and storm-specific feature, and typically do not explicitly consider the physical process. Some examples of major statistical models include the Climatology and Persistence model (CLIPER5), the Statistical Hurricane Intensity Forecast (SHIFOR), the Statistical Hurricane Intensity Prediction Scheme (SHIPS). Finally, ensemble or consensus models are a weighted average of individual forecast models. Major ensemble models include the Global Ensemble Forecast System (AEMN / AEMI), the UK Met Office model (UEMI), and the Florida State Super Ensemble (FSSE).

Due to the chaotic and complex nature of the energy exchange process between the sea and the atmosphere, and due to imperfect acquisition of real-time data, current operational TC forecasts cannot always provide sufficiently accurate and reliable guidance. For numerical methods, a significant weakness is insufficient representation of the complex dynamical process; however, increasing the number of variables or equations would lead to exponentially larger computational requirements. On the other hand, statistical methods, which are typically regression-based and less expensive computationally, may not capture effectively nonlinear relationships.

To address these issues, scientists have begun exploring deep learning (DL) techniques for hurricane forecasting. Indeed, DL is especially good at capturing the underlying nonlinear relationships using sophisticated models coupled with a wide variety of data, such as satellite, radar, and in-situ data, to improve TC forecast skills. For instance, Moradi Kordmahalleh et al. (2016) and Alemany et al. (2019) have used Recurrent Neural Networks for track forecasting by modeling it as a time series problem. Chen et al. (2019), Lian et al. (2020) and Giffard-Roisin et al. (2020) have demonstrated the potential of Convolutional Neural Networks and Recurrent Neural Networks to process historical statistical data and satellite imagery to make predictions.

This work introduces an ML framework, dubbed Hurricast (HURR), for intensity and track forecasting, which combines multiple individual forecasting approaches and several data sources. Our models can match the 24-hour lead time tracking performance of operational forecasts and outperform the best statistical-dynamical models in intensity by approximately 10%. In addition, we have created an ensemble model based on operational forecasts and Hurricast model that can outperform both FSSE and NHC's OFCL model in 24-hour lead time intensity and track forecasting.

The contributions of this paper are four-fold:

1. Presenting a new multimodal machine learning methodology for hurricane intensity and track predictions by combining multiple individual data sources: statistical features based on historical data, spatial-temporal features based on atmospheric reanalysis maps, and forecasts from currently operational models. We demonstrate improvement in prediction accuracy by combining data sources.
2. Based on our testing, ensemble models that include our machine learning model as an input can outperform all current operational models. This demonstrates the potential value of developing machine learning approaches as a new branch methodology for hurricane forecasting.
3. We demonstrate that a machine learning approach using boosted-tree-based methods (XGBoost) with advanced processing techniques, such as deep feature extraction from computer vision and deep learning, can outperform operational statistical-numerical models. Our tree-based methodology is particularly useful for combining data sources.
4. We introduce two encoder-decoder models, based on a Convolutional Neural Network encoder and a Gated Recurrent Units or Transformers decoder, combining statistical and vision data, that can perform TC spatial-temporal feature extraction. To the best of our knowledge, this is the first time a deep encoder-decoder architecture is explicitly compared to operational forecasts for TC track and intensity forecast at the same time and is concurrently used as a deep feature extractor. This is also the first time the success of a Transformer-decoder architecture is demonstrated in hurricane forecasting.

The paper is structured in the following manner: Section 2 outlines the current state of forecasting methods in the discipline; Section 3 describes the data used in the scope of this study; Section 4 elucidates the key challenges; Section 5 explains detailed methodologies to resolve these challenges, as well as the operational principles underlying our Machine Learning models; Section 6 describes the experiments conducted; Section 7 deals with conclusions from the results and validates the effectiveness of our framework.

2. Related Work

a. Numerical Methods

Numerical models, also known as dynamical models, are complex and computationally expensive numerical simulations. Forecasts are made by solving physical equations that model atmospheric dynamics using initial conditions based on observations, measures and geographical knowledge of the area. However, errors or uncertainties

around initialization grow as time evolves in the simulation, leading to increasingly inaccurate longer-time predictions. Moreover, the computational time is often a bottleneck to obtain near real-time forecasts, especially when reactivity is at stake.

One essential operational numerical model is the European Center for Medium-Range Weather Forecasting (ECMWF) model, developed by European member states, and is one of the most sophisticated and computationally expensive models. It runs twice daily, providing forecasts for all tropical cyclones across the globe up to 240 hours ahead. The calculation employs a hydrostatic spectral model, corresponding to a horizontal grid spacing of about 25 km (ECMWF 2019). Another important example is the Hurricane Weather Research and Forecasting (HWRF) model, developed by the National Centers for Environmental Prediction (NCEP) and operational since 2007. Unlike the ECMWF model, the HWRF model provides regional forecasts only for North Atlantic (NA) and Eastern Pacific (EP) basins. It is run at six-hour intervals with a prediction horizon up to 126 hours. The HWRF model employs an extensive range of data, including satellite observations, buoys and reconnaissance aircrafts (Biswas et al. 2018). Other important and currently operational numerical models include: the United Kingdom Meteorological Office (UKMET) model, the U.S. National Weather Service Global Forecast System (GFS) model, the Canadian Meteorological Centre (CMC) Global Environmental Multiscale Model (GEM), Limited Area Sine Transform Barotropic (LBAR) model.

b. Statistical Methods

Statistical approaches make predictions by modeling the historical relationships between storm-specific features, such as the time and location, and storm behavior. In comparison with numerical models, statistical models are computed more efficiently, albeit predictions are generally less accurate. Typically statistical models specialize in one of the forecasting tasks, either track or intensity.

The simplest form of statistical model is a regression-based model. An important example of such is the Climatology and Persistence Model (CLIPER5) developed in the 1970s. It provides track forecasts up to 120h ahead. It uses features including the successive displacements, the current latitude and longitude, the date, and the initial intensity (Knaff et al. 2003). A similar type of intensity forecasting model is the Statistical Hurricane Intensity Forecast (SHIFOR5) model, which uses climatology and persistence (Jarvinen and Neumann 1979). Due to these models' simplicity, they are often considered as "benchmark" models, compared to which the performance of more sophisticated models is evaluated.

A more sophisticated type of statistical model is the statistical-dynamical model, which, in addition to storm-specific features, uses predictive information obtained from dynamical models to approximate historical storm behavior. One important example is the Statistical Hurricane Intensity Prediction Scheme (SHIPS). SHIPS is based on standard multiple regression techniques using predictive features, including climatology and persistence, atmospheric environmental parameters (e.g., vertical shear, stability, etc.), and oceanic features such as sea surface temperature and upper-oceanic heat content (DeMaria and Kaplan 1994). The model is regularly updated as new data are collected; up to 2017, the SHIPS model is developed based on data from 1982 through 2006.

In addition, statistical models also include ensemble models, commonly called consensus forecasts. They are typically the weighted average of individual models or multiple runs of a single model. They are often able to outperform single models as they combine the strengths of different approaches (Wang et al. 2020; Lin et al. 2020), and the variation of individual models are used as a measure of forecast uncertainty. Many consensus models, such as the GUNS, GUNA and CGUN models, are produced by averaging guidance from chosen individual member models. A more sophisticated model is the Florida State University Super Ensemble (FSSE) model, which assigns different weights to each member model based on individual models' predicting power (Krishnamurti et al. 2011).

c. Machine Learning methods

Machine Learning models differentiate from traditional statistical models because they aim to use various data sources, such as satellite, radar, and in-situ data, to explicitly incorporate information arising from the physical process. In general, ML models combine physically-motivated information, storm-specific features and historical storm behavior to make predictions. Recent developments in Deep Learning (DL) enable ML models to employ multiple data processing techniques to process and combine information from a wide range of sources, and create sophisticated architectures to model spatial-temporal relationships. One such architecture is the neural networks, sometimes called artificial neural networks, a biologically-inspired paradigm from the human brain. Basic neural network types include recurrent neural networks (RNNs) — a type of architecture typically employed to process temporal or sequential data — and Convolutional neural networks (CNNs) — a type of computer vision technology employed to process spatial information. Tensor decomposition methods are another approach to process two and three-dimensional data. Finally, these individual architectures can be combined, using neural networks or tree-based methods, to make predictions.

1) NEURAL NETWORK-BASED MODELS

(i) *Recurrent Neural Networks* Recurrent Neural Networks (RNN) are a class of artificial neural networks that can model temporal dynamic behavior in time sequences. Their particular ability to recognize sequential characteristics and patterns in data makes them strong candidates for hurricane forecasting. In particular, two kinds of RNN could be useful: Long Short Term Memory (LSTM) (Hochreiter and Schmidhuber 1997) and Gated Recurrent Units (GRU) (Chung et al. 2014) that are specifically designed to handle long-term dependencies in sequential problems.

Several studies have demonstrated the use of RNNs to predict hurricane trajectory. Moradi Kordmahalleh et al. (2016) developed 6h and 12h forecasts based on historical trajectory data, and was tested on 4 tropical cyclones. Similarly, another model developed by Gao et al. (2018) was tested on Northwest Pacific tracks. Moreover, Alemany et al. (2019) developed a model using additional storm-specific features, such as the latitude, longitude, wind speed, and pressure to make 6-hour interval predictions over a 120-hour forecasting period. However, the predictive power of tabular trajectory data is limited while incorporating local meteorological field data is crucial for this complex problem.

(ii) *Convolutional Neural Networks* A significant portion of physical information is given by satellite imagery, and computer vision techniques emerge as well-suited solutions to process geo-spatial data. In particular, convolutional neural networks (CNN), a type of deep neural network, are one of the best architectures to analyze imagery data (LeCun et al. 1989; Krizhevsky et al. 2012; He et al. 2016).

Many studies have demonstrated CNNs' capabilities in modeling physical dynamical processes. For example, de Bézenac et al. (2017) demonstrate the predictive power of combining CNNs with physical knowledge to predict the evolution of sea surface temperature. Racah et al. (2016) applied CNN for automatic detection of extreme weather events like tropical cyclones from snapshots of the global atmospheric state available in CAM5 data set Neale et al. (2010).

Besides, Shi et al. (2015) introduced a Convolutional LSTM (ConvLSTM) model, by combining CNNs and RNNs, to make accurate precipitation forecasts, demonstrating capabilities in spatial-temporal modeling tasks. Sønderby et al. (2020) propose a Neural Weather Model based on ConvLSTM architecture, which forecasts rates of precipitation more accurately than dynamical models for up to 8 hours. These studies suggest deep learning architectures are promising, in general, to help with weather prediction and can successfully leverage meteorological field inputs in various forecasting and detection problems. Mudigonda et al. (2017) and Kim et al. (2019) applied

similar architectures for predicting hurricane trajectories using the CAM5 data set and historical storm tracks. Lian et al. (2020) applied a CNN and GRU architecture on location information and meteorological features for TC track forecasting.

Chen et al. (2019) and Su et al. (2020) respectively use reanalysis maps and satellite imagery to predict storm intensification and can outperform operational forecasts.

According to Chen et al. (2020), two of the most advanced deep learning methods in the literature for hurricane forecasting include Giffard-Roisin et al. (2020) for track forecasting and Chen et al. (2019) for intensity forecasting. They base their architectures on CNNs processing different kinds of meteorological data, in particular reanalysis maps extracted from ERA-Interim (Berrisford et al. 2011).

Giffard-Roisin et al. (2020) propose to concatenate the embeddings output by a CNN processing the reanalysis maps, with the embeddings of linear layers processing TC statistical data. These fused embeddings are then passed through a linear layer that then predicts hurricane trajectory. To model the dynamical nature of the system, two time steps of data (t and $t - 6h$) are stacked as different input for the CNN channels. However, this approach does not allow longer time-series as input and would show limits to make longer-term forecasts, as stacking time steps does not account for the temporal aspect. Their deep learning model performs better than the OFCL forecast until 2010 for the Eastern Pacific basin and 2006 for the North Atlantic basin.

Contrary to Giffard-Roisin et al. (2020), Chen et al. (2019) do not use statistical data but propose a hybrid CNN-LSTM architecture to model the dynamics. They show successful results in hurricane formation and intensity forecasting. They report an 18% better intensity prediction accuracy than the HWRF and SHIPS models in the EP basin and 3% worse in the NA basin. However, their comparison is made with the average error of operational forecasts between 2014 and 2018, and it is unclear if the performance of each model is reported on the exact same test set, and if the train/test separation was made in a leave-one-year-out fashion or random across the years, which is less realistic for deployment.

(iii) *Attention and Transformers* In the context of sequential data, and in particular Sequence-to-Sequence tasks, Attention mechanisms (Bahdanau et al. 2014) have successfully dealt with alignment issues — i.e., the fact that in Sequence-to-Sequence tasks, the input at time t over-dominates the t^{th} RNN's hidden representation — and RNN's difficulties to model long-range dependencies in a sequence. The idea is to learn a reweighted combination of a time series' hidden representations by allowing a receptive layer to "pay attention" to some specific parts of its inputs. It resulted in significant improvements in

most computational linguistics’ tasks such as translation or language modeling (Galassi et al. 2020). Not only is the method now ubiquitous in the field of Natural Language Processing (NLP), but also other ML sub-fields have applied attention mechanisms on images (Jetley et al. 2018) and meteorological data (Sønderby et al. 2020).

Based on attention mechanisms, Vaswani et al. (2017) proposed the Transformer, an encoder-decoder architecture relying solely on attention and obtaining state-of-the-art results on translation tasks specifically. This architecture has fostered considerable investigation from the NLP community with impressive results in language modeling tasks (Devlin et al. 2018; Liu et al. 2019; Lan et al. 2019; Brown et al. 2020). The success is mostly due to self-attention mechanisms, an extension of the initial attention mechanism where the attention is applied between input tokens only, in contrast with the original attention mechanism that assumes the existence of a “source” and “target” sequence. This makes computations easily parallelizable and efficient (see Appendix C for more details). Since then, Transformers have become the standard in Sequence modeling tasks with Deep Learning. Recently, Yun et al. (2019) demonstrated the general expressive power of Transformers on Sequence-to-Sequence tasks, which motivates the use of such architectures for hurricane forecasting. Applications of transformers on non-NLP sequential tasks are for now scarce but promising. They include in-hospital mortality (Oh et al. 2018), influenza prevalence (Wu et al. 2020), energy production and traffic forecast (Li et al. 2019). Transformers have also been applied to computer vision tasks such as classification (Jaderberg et al. 2015) or segmentation (Carion et al. 2020).

2) TREE-BASED METHODS

Tree-based algorithms are one of the best and mostly used supervised learning methods (Breiman et al. 1984; Bertsimas and Dunn 2017). They use a series of in-then rules to generate predictions from one or more decision trees. There are three main categories of tree-based models: decision trees, which are the foundation of all tree-based models; random forest, an “ensemble” method built upon many independent trees; gradient boosting trees, an “ensemble” built upon sequential trees. The latter two are popular choices for machine learning tasks, as they can reach high accuracy, stability and often offer good interpretability. Their capabilities to model non-linear relationships can lead to superior performance than linear models. For our project, we applied XGBoost (Chen and Guestrin 2016), which belongs to the gradient boosted tree framework, for its training speed and superior performance on our data set compared to the other tree-based methods mentioned.

3. Data

For this study, we use three kinds of data dated since 1980: historical storm data, reanalysis maps, and operational forecasts data from the NHC. Among all the tropical cyclones, we selected those with maximum sustained wind speed reaching at least 34 knots at some time t_0 and containing at least 60 hours of record after this time t_0 . The three types of data are matched according to storm ID and date-time criteria.

a. Historical Storm Data Set

We obtained historical storm data set from the National Oceanic and Atmospheric Administration (Knapp et al. 2010). Among the available features, we have selected the latitude, the longitude and the pressure at the center of the hurricane, the maximum sustained wind speed from the WMO agency (or from the regional agency when not available) for the current location, the distance-to-land, the translation speed of the hurricane, the direction of the hurricane (in degrees), the nature of the storm and the basin (North-Atlantic, Eastern Pacific, Western Pacific, etc). The choice of these features is consistent with previous statistical forecasting approaches (DeMaria and Kaplan 1994; Shimada et al. 2018; Giffard-Roisin et al. 2020). In this paper, we will refer to this data as *statistical data*.

b. Reanalysis Maps

Reanalysis is a scientific method to produce a comprehensive record of how weather and climate evolve over time. As the name suggests, the reanalysis maps consist of numerical aspects of the Earth systems, such as the air pressure, humidity, wind speed, based on satellite observations and numerical analysis, covering the entire globe from the surface level to the atmosphere above. The reanalysis maps are used extensively for atmospheric monitoring, climate research, and climate predictions. For our project, we use the ERA-5 reanalysis data set, developed by the ECWMF, which is one of the most extensive and contains high spatial resolution reanalysis data sets from 1979 to the present (ERA5 2017). Our choice of data set is inspired by previous machine learning works (Chen et al. 2019), (Giffard-Roisin et al. 2020).

We extracted ($25^\circ \times 25^\circ$) maps centered at the storm location, of resolution $1^\circ \times 1^\circ$, i.e., each cell corresponds to one degree of latitude and longitude, offering a sufficient frame size to capture the entire storm. We obtained nine reanalysis maps for each time step, corresponding to three different features, geopotential z , u and v components of the winds, at three atmospheric altitudes, 225, 500, and 700hPa (see Figure 1). The three features’ choice is motivated by the physical understanding that wind direction and geopotential differences highly determine the hurricane evolution. The motivation to use data from three

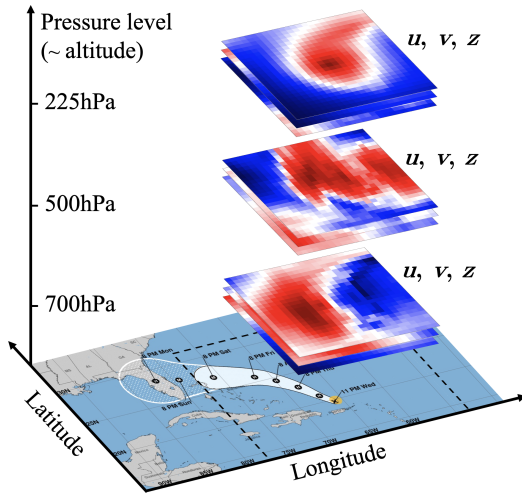


FIG. 1. Representation of the 9 reanalysis maps extracted for each time step, corresponding to geopotential z , u and v components of the winds, repeatedly extracted at three atmospheric altitudes, 225, 500, and 700hPa. Each map is of size $25^\circ \times 25^\circ$, centered on the eye of the hurricane, and each pixel corresponds to the average field value at the given latitude and longitude degree.

different atmospheric altitudes is to capture the air movements at different levels of the troposphere, corresponding to low, mid and high clouds, since wind fields are the direct observations of the atmospheric flows. The choice of these 3 features and 3 levels aligns with previous studies (Shimada et al. 2018; Chen et al. 2019; Giffard-Roisin et al. 2020).

c. Operational Forecast Models

In addition to historical storm data and reanalysis maps, we have further included operational forecasts. The operational forecast data is obtained from the HURDAT2 data set, maintained by the National Hurricane Center (NHC) (Landsea et al. 2015). The HURDAT2 data contains historical forecasts for tropical cyclones and subtropical cyclones in the North Atlantic and Eastern Pacific basins, by operational models used by the NHC for its official forecasting. Among available operational models, we have selected values from Climatology and Persistence Model (CLP5), Statistical Hurricane Intensity Prediction Scheme (SHIP), SHIPS with Inland Decay (DSHP), Global Forecast System (GFSO), Limited Area Barotropic Model (LBAR), Environment Canada Global Environmental Multiscale Model (CMC), Geophysical Fluid Dynamics Laboratory Model (GFDL), Hurricane Weather Research and Forecasting Model (HWRF), United Kingdom Met Office Model (UKXI), Florida State University Super-Ensemble (FSSE), National Weather Service Global Ensemble Forecast System (AEMN), Official NHC Forecast (OFCL). From each of these models, we included four forecasted features: latitude, longitude, maximum sustained wind

speed, and minimum sea level pressure. The implementation of the data extraction is done using the Tropical Python package (Burg and Lillo 2020), which obtains data from the HURTDAT2 data set (Landsea et al. 2015).

4. Problem Formulation

Our project aims to obtain accurate TC forecast using a machine learning approach utilizing a wide range of data including historical storm-specific data, satellite map data, and operational forecast models' predictions. Based on the diverse source of data, we aim to develop a spatial-temporal model that takes into account both the physical process and the statistical behavior. To achieve this goal, we identify three main challenges: 1) spatial (vision) data processing, 2) temporal data processing, 3) data fusion. In the following subsections, we expand on each challenge and briefly outline our methodologies for addressing them. The precise methodology is detailed in Section 5.

a. Challenge 1: Spatial Data Processing

Reanalysis maps give important information regarding the physical dynamics of the storm. Each map for one particular variable at a fixed time step is a two-dimensional matrix, each axis corresponding to latitude and longitude. Then, as we use reanalysis maps at different pressure levels, the reanalysis feature maps forms a three-dimensional tensor for each time step. Each pixel in the map thus corresponds to one of the variables at a given pressure level. Such format of information can be well-suited for numerical simulations; however, it cannot be processed directly by standard statistical learning methods. To solve this challenge, we need to convert spatial-temporal data into one-dimensional data through feature extraction.

In particular, we propose two different techniques to extract reanalysis maps embeddings: using a supervised learning fashion with encoder-decoder network architectures (see 5.b.1) or using an unsupervised fashion with tensor decomposition methods (see 5.b.2). The spatial-temporal features extracted can then be used along with statistical features to train standard machine learning algorithms, such as tree-based models.

b. Challenge 2: Temporal Data Processing

Temporal modeling of physical phenomena comes intrinsically with dynamical equations; however, the sequential modeling of time series data remains a challenging task for machine learning algorithms. In our models, for a specific prediction at a lead time of 24 h, we use a fixed sequence size of the past 21 h of corresponding TC data (i.e., 8 time steps spaced at a 3 h frequency). Then we can use recurrent neural networks or attention mechanisms with positional encoding (Vaswani et al. 2017) and sophisticated tree-based models like XGBoost to capture the

nonlinear and temporal relationships between each time step of the sequence.

c. Challenge 3: Data Fusion

Using a wide range of data sources naturally leads to the question of data fusion. In particular, we need to build one model which can process and make predictions based on data with a wide range of formats and dimensions. For example, the reanalysis maps sequences are spatial-temporal four-dimensional data, while historical storm data sets are vectorized one-dimensional data. Besides, storm-specific features can have various formats; for instance, the basin is a categorical feature, longitude and latitudes are geographical features, wind speed is a numerical feature, date and time are temporal features, wind direction is a periodical numerical feature.

To solve this challenge, we demonstrate that by concatenating processed and engineered features from each data source, a tree-based model can efficiently capture the complex correlations between them. This means we build a one-dimensional vector, joining each set of features from each different source, to form a single entry for our tree-based models.

5. Methodology

In summary, we adopt a three-step approach: first, we process each data source — statistical data, reanalysis maps or operational forecasts — with the relevant methodology. Second, we concatenate all the processed features in a one-dimensional format and perform feature selection. Third, we make our predictions using a tree-based model trained on the selected data. At a given time step, we perform two 24-hour lead time forecasts: an intensity prediction task, i.e., predicting the intensity of the storm at forward 24-hour time; a displacement regression task, i.e., predicting the latitude and longitude storm displacement in degrees between given time and forward 24-hour time. Figure 2 serves as an illustration of the three-step pipeline.

We explore several combinations of data to determine the best model. The structure of this section is as follows: first, we discuss our various techniques for processing statistical and vision data (reanalysis maps); then, we discuss the technique for data fusion and finally the prediction.

a. Statistical Data Processing

The statistical data described in Section 3.a is processed through several steps in order to later engineer useful features for tree-based models.

First, categorical features are treated using the one-hot encoding technique. For a specific categorical feature, each possible category is converted as an additional feature, with 1 indicating data set belonging to this category and 0

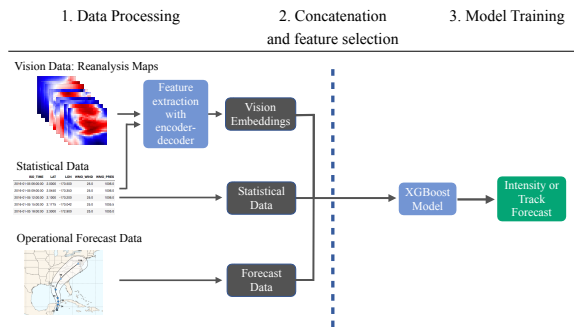


FIG. 2. Representation of our multimodal machine learning framework using all three data sources: statistical, reanalysis maps, and operational forecast values. During Step 1, data are processed individually to produce features using corresponding techniques. See Section 5.a and 5.b for further details. In particular, we can use our encoder-decoder architectures to perform a spatial-temporal feature extraction from reanalysis maps and statistical data. During Step 2, we concatenate a combination of features and perform feature selection. See Section 5.c for further details. During Step 3, we train one XGBoost model for each prediction task: intensity in 24 h, latitude displacement within 24 h, and longitude displacement within 24 h. See Section 5.d for further details.

otherwise. We encode the basin and the nature of the TC as one-hot features.

Second, cyclical features are encoded using cosine and sine transformations to avoid singularities at endpoints. Features processed using this smoothing technique include date, latitude, longitude, and storm direction.

Third, missing values are treated using a linear interpolation method. The issue of missing values in our data set only concerns maximum sustained wind speed and pressure features. Indeed, these variables are sometimes recorded at a 6-hour frequency, while the track was recorded at a 3-hour frequency. For our model, we chose a 3-hour time step frequency to provide higher training granularity.

Finally, we have engineered additional features to capture first-order dynamical effects. In particular, we compute the latitude and longitude displacement between consecutive steps.

b. Vision Data Processing

We have experimented with two computer vision techniques to perform feature extraction from reanalysis maps: (1) encoder-decoder networks and (2) tensor decomposition methods. The former is a supervised learning method; for each input, there is an associated labeled value as prediction target. We report in particular about two specific encoder-decoder architectures: a CNN-encoder GRU-decoder and a CNN-encoder Transformer-decoder. On the other hand, the tensor decomposition is an unsupervised method; there is no specific labeled prediction target and instead predictions are drawn directly from the patterns

within the data. In the following subsections, we provide outlines for each method.

1) ENCODER - DECODER ARCHITECTURE

We perform two approaches based on the encoder-decoder architectures: (i) directly predict TC intensity and track, (ii) once the network is trained, extract low-dimensional reanalysis maps embeddings as features to be input into tree-based methods.

As the name suggests, the architecture consists of a CNN component acting as an encoder, and either a GRU or a Transformer component acting as a decoder. The CNN component aims to process (embed) the reanalysis maps. The GRU aims to model the temporal aspect through a recurrence mechanism, while the Transformer utilises attention mechanisms and positional encoding to model long-range dependencies more effectively. In contrast with the GRU that processes the input sequentially, the Transformer's self-attention layer allows a given output to be a function of the entire sequence. Therefore, there is no "sequentiality" anymore and the inherent sequential aspect of the data is reintroduced with the positional encoding.

Figure 3 and 4 serve as an illustration of the encoder-decoder architectures, and more details on all components are given in Appendix C.

(i) *Predict TC intensity and track* To make a 24-hour lead time forecast, we use a fixed historical window size of past 21-hour data, corresponding to 8 distinct 3-hour frequency time steps in the data set.

The CNN-encoder At each time step, the corresponding 9 reanalysis maps (see Section 3.b) are fed into the CNN-encoder, which produces lower-dimensional embeddings. The CNN-encoder consists of three convolutional layers, with ReLU activation and MaxPool layers in between, then followed by two fully connected layers (see Appendix C for exact architecture).

Next, we concatenate the reanalysis maps embeddings with processed statistical data corresponding to the same time step. Note that at this point we still have an 8-time step sequence of concatenated features. The way this sequence is handled by the GRU-decoder or the Transformer-decoder is slightly different and we detail the process in the two following paragraphs.

The GRU-decoder Our GRU-decoder consists of two unidirectional layers. According to the chronological order, the previous data is fed sequentially into the GRU-decoder to reflect the temporal aspect. For each time step, the GRU-decoder outputs a hidden state representing a "memory" of the previous time steps. Finally, a track or intensity prediction is made based upon these hidden states concatenated all together and given as input to fully-connected layers (see Figure 3).

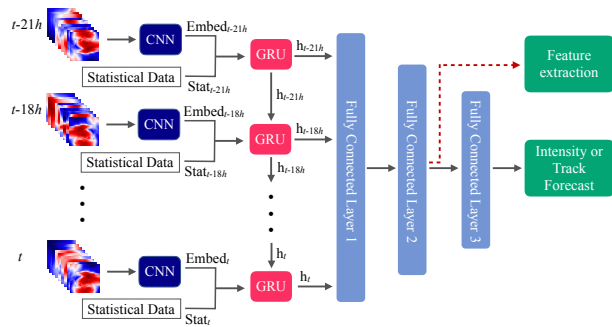


FIG. 3. Representation of our CNN-encoder GRU-decoder network for an 8-time step hurricane sequence. At each time step, we utilize the CNN to produce one-dimensional embeddings of the reanalysis maps. Then, we concatenate these visual embeddings with the corresponding statistical features to create a sequence of inputs fed sequentially to the GRU. At each timestep, the GRU outputs a hidden state that is also passed to the next time step. Finally, we concatenate all the successive hidden states and pass them through 3 fully connected layers to predict intensity or track with a 24-hour lead time. Spatial-temporal embeddings can be extracted as the output of the second fully connected layer.

The Transformer-decoder Conversely to the GRU-decoder, the sequence is fed as a whole into the Transformer-decoder. Since the attention mechanism allows each hidden representation to attend holistically to the other hidden representations, the time-sequential aspect is lost. Therefore, we add a *positional encoding* token at each timestep-input, following Vaswani et al. (2017). Adding this token that represents the relative position of a token within the sentence re-injects some information about the inherent sequential aspect of the data and experimentally improves performances (see Appendix C for details).

Then, we use 2 layers of Transformer's encoder that transforms the 8 timesteps (of size 142) into an 8-timestep sequence with similar dimensions. To obtain a unique representation of the sequence, we average the output sequence feature-wise into a one-dimensional vector, following standard practices. Finally, a track or intensity prediction is made based upon this averaged vector input into one fully-connected layer (see Figure 4).

Training process We train the aforementioned encoder-decoder architectures in an end-to-end fashion, using standard backpropagation to update the weights parameterizing the model (Rumelhart et al. (1985), Goodfellow et al. (2016)). We use a mean squared error loss with either an intensity or track objective and add an $L2$ regularization on the weights of the network (see Appendix C for further details). The intensity objective consists in predicting the maximum sustained windspeed in 24 hours (one value to predict). The track objective consists in predicting the total displacement between the current instant and the next 24 hours (two values to predict, the latitude and longitude displacements in degrees).

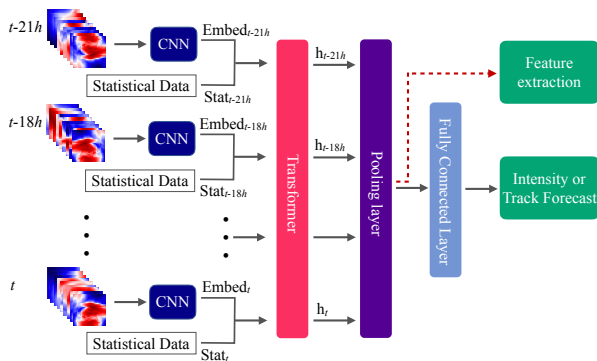


FIG. 4. Representation of our CNN-encoder Transformer-decoder network for an 8-time step hurricane sequence. At each time step, we utilize the CNN to produce one-dimensional embeddings of the reanalysis maps. Then, we concatenate these visual embeddings with the corresponding statistical features to create a sequence of inputs fed as a whole to the Transformer. The Transformer outputs a new 8-timestep sequence that we average (pool) feature-wise and then feed into one fully connected layer to predict intensity or track with a 24-hour lead time. Spatial-temporal embeddings can be extracted as the output of the pooling layer.

Comparison of our encoder-decoders with related work Giffard-Roisin et al. (2020) employed a similar CNN architecture for track forecast, using statistical data and reanalysis maps, but did not use any decoder component, and thus not accounting for the temporal aspects of the data. Besides, the intensity forecasting task was not explored in their work. Chen et al. (2020) used a hybrid CNN-LSTM network for hurricane formation and intensity forecasting but did not explore track forecasting or augmented their models with statistical data. None of these two approaches explored feature extraction from neural networks, and to the best of our knowledge, our work is the first benchmark on this methodology for TC forecasting.

(ii) *Feature extraction* We designed the encoder-decoder architectures to perform well in TC intensity and track forecasting, as explained in 5.1.(i), and provide predictive and low-size embeddings of the reanalysis maps. We now describe how we extract these embeddings and then explain the motivation behind this extraction.

We use the same format of inputs and pipeline as before and we train the whole network with the same data and objective as before (intensity or track). Then, we freeze the encoder-decoder’s weights after training is completed. Next, given an input sequence of reanalysis maps and statistical data, we pass them through the whole network, in the same fashion as before, except from the last fully-connected layer (see Figure 3 and 4). The second fully connected layer after the GRU or the pooling layer after the Transformer output a vector of relatively small size, e.g., 128 features, to compress information and provide more predictive features

for our following tree-based methods. This vector constitutes our one-dimensional reanalysis maps embedding that we extract from the initial 45,000 ($8 \times 9 \times 25 \times 25$) features forming the spatial-temporal input.

The motivation of this extraction lies in the hope that while the encoder-decoder acquired intensity or track prediction skills during training, it captures relevant embeddings of the reanalysis maps. Using these internal features as input to an external model is a method inspired by transfer learning and distillation generally efficient in visual imagery (Yosinski et al. 2014; Kiela and Bottou 2014; Tan et al. 2018; Hinton et al. 2015). Another interest is the ability to turn a four-dimensional spatial-temporal tensor into a one-dimensional vector, that can serve as practical input in a tree-based method. Finally, the framework also captures correlations between vision and statistical data. Indeed, the spatial-temporal embeddings were obtained through combining reanalysis maps and statistical data within the network just before the GRU or Transformer (see Figures 3 and 4).

2) TENSOR DECOMPOSITION

In addition to using encoder-decoders to extract embeddings from the reanalysis maps, we also explored tensor decomposition methods. A tensor is a multidimensional linear algebraic object; for instance, a one-dimensional tensor is a vector, and a two-dimensional tensor is a matrix.

Tensor analysis is commonly used in signal processing to compress and de-noise high dimensional tensors using low dimensional tensors and projection maps (Kolda and Bader 2009; Sidiropoulos et al. 2017). In addition, Yan et al. (2014) show such decomposition techniques can be applied to perform feature extraction tasks from imagery data, and Chen et al. (2018) show that a specific type of Tucker decomposition demonstrates capabilities to capture spatial-temporal relationships. Figure 5 exhibits a geometric representation of the Tucker decomposition applied to a three-dimensional tensor \mathcal{A} , which is decomposed as a smaller core tensor \mathcal{S} and projection maps $U_{i=1,2,3}^i$.

For this project, at each time step, we treat reanalysis maps over past time steps as a four-dimensional tensor, of size $8 \times 9 \times 25 \times 25$ (corresponding to 8 past time steps of 9 reanalysis maps of size 25 pixels by 25 pixels), and used the core tensor obtained from the Tucker decomposition as extracted features. The decomposition is achieved using the multilinear singular value decomposition (SVD) method, which is a computationally efficient method (De Lathauwer et al. 2000). Finally, the core tensor is flattened and can be concatenated with the corresponding statistical features to train tree-based methods. More details on tensor decomposition methodology can be found in Appendix C.

As a remark, the size of the core tensor, i.e., the Tucker rank of the decomposition, is a hyperparameter to be tuned.

Based on validation, the Tucker rank is tuned to size $3 \times 5 \times 3 \times 3$ (see Section 6 for more details).

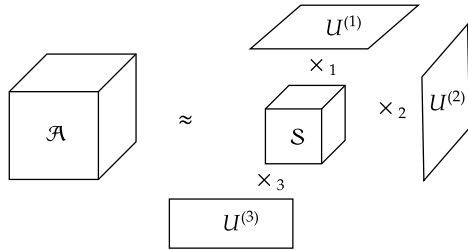


FIG. 5. Illustration of the tensor decomposition of a 3 dimensional tensor. Tensor \mathcal{A} is the original tensor, which is approximated through Tucker decomposition using a core tensor \mathcal{S} and three linear projection maps along each axis $U^{(1)}$, $U^{(2)}$, $U^{(3)}$.

c. Concatenation and feature selection

Now that we explained how we can extract one-dimensional embeddings from reanalysis maps, we outline the methodology to combine all data sources together. First, we describe how we concatenate all features and then how we perform feature selection.

(i) *Concatenation of the data* Different data are available: statistical data (see 5.a), reanalysis maps embeddings extracted from the encoder-decoder (see 5.b.1) or from the tensor decomposition (see 5.b.2), and operational forecasts (see 3.c). Depending on which data sources to use, we concatenate the relevant sets to form a one-dimensional vector.

First, we concatenate the whole statistical data sequence corresponding to the fixed window size of past observations into a one-dimensional vector. As a result, the time-sequential aspect of the features is no longer explicitly defined, and instead, we rely on sophisticated tree-based models to learn the complex non-linear dynamics.

As previously mentioned, we have used the past 21 hours of data, corresponding to 8 time steps, as the fixed window size. The historical range is chosen based on validation accuracy (details in Section 6.c).

Second, if the specific variation of the model includes vision data, we extract the visual embeddings from the reanalysis maps sequence using either the encoder-decoder (see 5.b.1) or the tensor decomposition (see 5.b.2). Therefore, for each visual sequence, we get a one-dimensional embedding vector that characterizes the whole spatial-temporal time series. This vector is then concatenated to the previous statistical data vector, as additional features.

Finally, if the specific variation of the model includes operational forecast data, we concatenate this one-dimensional vector with the sequence of operational forecast values available, corresponding to the eight successive 24-hour lead time forecasts.

Once all required data are concatenated, we perform feature-wise standardization for each feature, i.e., subtracting the mean and dividing by the standard deviation, to rescaling features towards mean 0 and standard deviation 1.

(ii) *Feature Selection* After concatenating the different data sources, the training data set amounts to about 200-1000 features. This relatively large number can provoke overfitting and longer training time. Thus, it is important to select the most relevant features before training and obtain stronger and more informative entries to our model. To do so, we employed the InterpretableAI software based on exact sparse linear regression (Bertsimas et al. 2019; Bertsimas and Van Parys 2020). After feature selection, the data is ready to train tree-based models for predicting the intensity and track location at a lead time of 24 h.

d. Summary of Models

In the scope of this work, we have experimented with various architectures based on different input data sources to make intensity and track forecasting. In this subsection, we list all the forecast models tested and retained, and provide a summary of the methodologies employed during the processing and training stages. We review these Hurricast models in Table 1.

Model 1 and 2 utilize vision data (reanalysis maps) coupled with statistical data, employing neural networks only with the encoder-decoder architecture detailed in Section 5.b.1. Both models employ a CNN-encoder architecture, but Model 1 employs GRUs as decoder while Model 2 employs Transformers as decoder.

Models 3-7 are variations of the three-step framework described in Figure 2, with the variation of input data source or processing technique. Model 3, HURR-(stat,xgb), has the most simple form, utilizing only statistical data. Model 4-6 utilize statistical data and vision data. They differ on the extraction technique used on reanalysis maps. Model 4, HURR-(stat/viz,xgb/td), uses vision features extracted with tensor decomposition technique (see 5.b.2), whereas Model 5 and 6 utilize vision features extracted with the encoder-decoder (see 5.b.1), with GRU and Transformer decoders respectively. Model 7, HURR-(stat/viz/op, xgb/cnn/gru/transfo), which has the most extensive form, utilizes statistical data, vision features extracted with both encoder-decoder architectures, and operational forecast data. Finally, Model 8 is a Lasso consensus model using operational forecasts and Model 6 forecasts.

We experimented with a consensus model to explore whether the Hurricast framework can bring additional benefits to current operational forecasts. We have chosen to use the variation Model 6 specifically, HURR-(stat/viz, xgb/cnn/transfo), as it is the most extensive form of Hurricast that does not use operational forecasts as input

TABLE 1. Summary of the various versions of the Hurricast framework for which we report results. Models differ in architecture and in data used. The data used can be a subset of statistical, vision (reanalysis maps embedded or not), and operational forecasts. For this reason, models are named based on two characteristics: the data used, and the methods used.

N°	Name	Data Used	ML Methods
1	HURR-(viz, cnn/gru)	Vision, Statistical	CNN, GRU
2	HURR-(viz, cnn/transfo)	Vision, Statistical	CNN, Transformers
3	HURR-(stat, xgb)	Statistical	XGBoost
4	HURR-(stat/viz, xgb/td)	Statistical, Vision embeddings	XGBoost, Tensor decomposition
5	HURR-(stat/viz, xgb/cnn/gru)	Statistical, Vision embeddings	XGBoost, CNN, GRU
6	HURR-(stat/viz, xgb/cnn/transfo)	Statistical, Vision embeddings	XGBoost, CNN, Transformers
7	HURR-(stat/viz/op, xgb/cnn/gru/transfo)	Statistical, Vision embeddings, Operational forecasts	XGBoost, CNN, GRU, Transformers
8	Lasso consensus op/HURR	Operational forecasts, HURR-(stat/viz, xgb/cnn/transfo)	Lasso

data. We chose Lasso (Tibshirani 1996) as a proof-of-concept consensus method for two reasons: (i) it is interpretable and straightforward, (ii) it makes predictions by selecting the relevant forecasts with a regularization term to ensure sparsity. In other words, if Hurricast could not offer insights in addition to currently operational forecasts, its associated weight would be set to zero.

We provide further details on the performance of these different models in comparison with operational forecasts in the following Section 6.

6. Experiments

In this section, we first describe our metrics for evaluating the models. We then explain our training, validation, and testing protocols and finally give the best combinations of hyperparameters found.

a. Evaluation metrics

We make two types of comparisons: (i) the standalone performance of our Hurricast models described in Table 1; (ii) the performance of operational forecasts consensus using or not Hurricast predictions.

To evaluate our intensity forecasts’ accuracy, we compute the mean average error on the predicted 10min-maximum sustained wind speed in 24 hours, defined as:

$$\text{MAE} := \frac{1}{N} \sum_{i=1}^N |y_i^{\text{true}} - y_i^{\text{pred}}|,$$

where N is the number of predictions, y_i^{pred} the predicted forecast intensity with a lead time of 24 h and y_i^{true} the ground-truth 10-min maximum sustained windspeed value given by the WMO agency.

To evaluate our track forecasts’ accuracy, we compute the mean geographical distance error in kilometers between

the actual position and the predicted position in 24h, using the Haversine formula. The Haversine metric (see Appendix C for the exact formula) calculates the great-circle distance between two points — i.e., the shortest distance between these two points over the Earth’s surface.

b. Training, Validation and Testing protocol

We now describe our model training, validation and testing protocol. In ML, the train set is used to fit the model’s weights on the data, the validation set is used to validate the hyperparameters choice, and the test set is used to provide an unbiased evaluation of the final trained model. We first explain how we split the data set, then describe the test set and testing methodology in larger details. Finally, we discuss the adjustments required to train the specific Hurricast models 5-6 that use operational forecasts.

1) DATA SET SPLIT

While our total data set comprises more than 3000 TCs from 6 different basins, we only keep those which reach a speed of 34 kn at some time, i.e., are classified at least as a Tropical Storm on the Saffir-Simpson hurricane wind scale, and where more than 60 h of data are available after they reached the speed of 34 kn for the first time. Then, we separate the data set into training (80% of the data), validation (10% of the data) and testing (10% of the data). The training set ranges from 1980 to 2011, the validation set from 2012 to 2015, and the test set from 2016 to 2019. Within each set, all samples are treated independently.

For models 1-4, we use data from all basins during training, but we only validate and test on the North Atlantic and Eastern Pacific basins, where we have benchmarks available. Based on empirical observation, models trained on TCs from all basins yield better performance than models trained on specific basins, even if the testing set restricts to a specific basin. One hypothesis could be there are common

patterns shared by TCs from all basins, and that cross-basin learning allows machine learning models to grasp such patterns. Besides, training on a larger amount of data may bring more generalization capacity to our models.

2) DESCRIPTION OF THE TEST SET

The test set comprises all the storm time steps between 2016 and 2019 from the NA and EP basins where operational forecast data is available, to be used as benchmarks to evaluate our models. In particular, we have selected the following operational forecasts as benchmarks based on availability and performance: SHIPS, Decay-SHIPS, GFSO, HWRF, FSSE and OFCL for the intensity forecast; CLP5, Decay-SHIPS, HWRF, GFSO, AEMN, FSSE and OFCL for the track forecast. We provide a summary of these models with their type and name in Table 2.

3) TESTING METHODOLOGY

We employ the validation set to perform hyperparameter tuning, i.e., finding the best combination of hyperparameters. Then, using tuned hyperparameters, we retrain the models on the training and validation set combined. We evaluate our models' performance year by year; in particular, for a particular testing year, we train and validate models using data before the testing year. For example, to evaluate prediction accuracy in 2018, models are trained and validated using data available up to the end of 2017, and tested performance using data in 2018. This process is repeated year by year to reflect the realistic scenario where models can be retrained every year using the latest data available.

For both intensity and track forecasts, we report the performance obtained on the NA and EP test set with each method, for 24-hour lead time forecasts. Tables A3 and A4 summarize the results for intensity forecasting and Tables A5 and A6 summarize the results for track forecasting.

We report performance in the last three consecutive years where testing data is available, i.e., 2017-2019 for the NA basin and 2016-2018 for the EP basin. Testing years for NA and EP differ because we did not have sufficient EP operational forecast values for comparison in 2019.

4) THE SPECIFIC PROTOCOL FOR MODELS USING OPERATIONAL FORECASTS

Operational forecast data is substantially available only after the year of 2012. As a result, when including operational forecast data as an input source, we need to make adjustments to the training procedure to accommodate missing values prior to 2012, to not compromise the number of training years. This issue arises specifically for two variations: the HURR-(stat/viz/op-xgb/nn) and Lasso consensus models. Therefore, we employ the following training methodology adjustment.

For the HURR-(stat/viz/op-xgb/nn) model, the model is trained using only data from 2012 onwards among all data sets. For instance, to evaluate the model performance using 2016 as a testing year, first, we train the XGBoost model using statistical data, vision embeddings and operational forecast from 2012 to 2014. During this training phase, we do not treat missing forecast data because XGBoost is able to intake *NaN* values. Then, we tune the hyperparameters of the XGBoost model using data in 2015 as the validation set. Next, we retrain the XGBoost model using data from 2012 to 2015 using validated hyperparameters. Finally, we test the performance in 2016. Similarly, such procedure is employed to evaluate other testing year performances by shifting the training, validation, and test set accordingly.

For the Lasso consensus model, we use the HURR-(stat/viz, xgb/nn) model trained upon data until 2012. To evaluate the model performance using 2016 as a testing year, first, we train a Lasso regressor based on predictions produced by HURR-(stat/viz, xgb/nn) and operational forecasts, where available, on the years 2012-2014. Then, we tune the Lasso regularization parameter using data in 2015. Then, the Lasso model is retrained using data from 2012 to 2015 with the tuned regularization parameter. Finally, the Lasso consensus performance is tested using data in 2016. Similarly, we repeat this process for other testing years, by shifting the training, validation and test set accordingly.

c. Hyperparameter Tuning

In this subsection, we provide the list of hyperparameters and the best configurations based on validation. We distinguish three categories of hyperparameters to tune: (1) the data-related features, (2) the neural-network related features, (3) the tensor decomposition-related features and (4) the tree-based method related features.

1) DATA RELATED FEATURES

The data-related features include the size of the reanalysis maps and the number of historical time steps of data to use for each forecast. We tune these features comparing the 24-hour lead time forecast performance of the encoder-decoders for each different hyperparameter configuration.

We found that using eight past time steps (i.e., up to 21 h in the past) and a grid size of 25×25 degrees (in fact, the whole grid size we extracted initially) for the reanalysis maps was the best combination. We also found that standardizing the vision and statistical data — i.e., rescaling each feature to mean 0 and standard deviation 1 — yielded better results than normalizing — i.e., rescaling each feature to the $[0, 1]$ range.

2) NEURAL NETWORK-RELATED FEATURES

The neural network-related features include the optimizer, the architecture itself, the batch size during train-

TABLE 2. Summary of all operational forecast models included in our benchmark.

Model ID	Model name or type	Model type	Forecast
CLP5	CLIPER5 Climatology and Persistence	Statistical (baseline)	Track
SHIPS	Statistical Hurricane Intensity Prediction Scheme	Statistical-dynamical	Intensity
Decay-SHIPS	Decay Statistical Hurricane Intensity Prediction Scheme	Statistical-dynamical	Intensity
GFSO	Global Forecast System model	Multi-layer global dynamical	Track, Intensity
HWRP	Hurricane Weather Research and Forecasting model	Multi-layer regional dynamical	Track, Intensity
AEMN	GFS Ensemble Mean Forecast	Consensus	Track
FSSE	Florida State Super Ensemble	Corrected consensus	Track, Intensity
OFCL	Official NHC Forecast	Consensus	Track, Intensity

ing, and the loss function’s regularizer. Recall that we have two downstream tasks for the neural network: an intensity regression task which consists of predicting the intensity of the storm in 24 h, and a displacement regression task which consists in predicting the latitude and longitude displacement of the storm in degrees between an instant t and $t+24$ h.

For both tasks, the best results were obtained using a batch size of 64, a λ regularization term of 0.01, and the encoder-decoder architectures described in Appendix C. Regarding the optimizer, we use Adam (Kingma and Ba 2014) with a learning rate of 10^{-3} for the intensity forecast and $4 \cdot 10^{-4}$ for the track forecast.

3) TENSOR DECOMPOSITION FEATURES

The tensor decomposition algorithm includes the choice of the core tensor size, i.e., the compressed size of the original tensor. Recall that the original tensor size is $8 \times 9 \times 25 \times 25$. Based on empirical testing, we found using a small tensor size of $3 \times 5 \times 3 \times 3$ yielded the best performance when compressed reanalysis maps are included as features in tree-based prediction methods.

4) TREE-BASED METHOD FEATURES

Based on empirical testing, we find XGBoost models outperforming consistently Decision Trees and Random Forests or other ML methods such as Support Vector Machines or regularized linear regression. XGBoost trains also fast which is a considerable advantage for heavy hyperparameter search. Therefore, we select XGBoost as the core model for prediction. Then, there is variability in the best combinations of hyperparameters depending on each task (track or intensity), basin (NA or EP) or data sources to use (statistical, reanalysis maps embeddings, operational forecasts). However, these particular features were typically important and were the best in the following ranges: maximum depth of the trees (between 6 and 9),

number of estimators (between 100 and 300), learning rate (between 0.03 and 0.15), subsample (between 0.6 and 0.9), column sampling by tree (between 0.7 and 1), minimum child by tree (between 1 and 5).

d. Computational resources

All our code is in Python 3.6 (Van Rossum and Drake Jr 1995). Neural networks are coded using Pytorch (Paszke et al. 2019). We train all our models using one Tesla V100 GPU and 6 CPU cores. Typically, our encoder-decoders train within an hour, reaching the best validation performance after 30 epochs. Our XGBoost models train within two minutes. The testing time is within a second, which shows practical interest if our models were to be deployed. The bottleneck would therefore lie in the acquisition of the reanalysis maps only.

7. Results

This section proves the four contribution claims made in the introduction, based on results derived from our experiments. Performance tables can be found in Appendix A and B for both basins and tasks.

(i) Successful combination of diverse data sources leads to more accurate forecasts than using single data sources.

Under the scope of this work, we report about seven variations of the Hurricast framework (see 5.d for a summary of variations). The distinctions are based upon variations in data sources and variations in machine learning techniques. Considering variations in data sources, we can group models into: 1) HURR-(stat,xgb) using only statistical data; 2) HURR-(viz, cnn/gru), HURR-(viz, cnn/transfo), HURR-(stat/viz, xgb/cnn/gru), HURR-(stat/viz, xgb/cnn/transfo), HURR-(stat/viz, xgb/td) using statistical and vision data (embedded or not); 3) HURR-(stat/viz/op, xgb/cnn/gru/transfo), using statistical, vision

embeddings and operational forecast data. As shown in Tables A3-A6, accuracy improves generally as models include more data sources. Such effect is especially clear when comparing the variation using one single source with the variations using all three data sources, e.g., comparing HURR-(stat,xgb) with HURR-(stat/viz/op, xgb/cnn/gru/transfo).

We show that extracting embeddings from multimodal encoder-decoder architectures is particularly useful and outperforms the original encoder-decoder architecture. This suggests the additional value from using tree-based models that have the capacity to combine efficiently diverse data sources. Therefore, we prove that combining different machine learning techniques is a promising framework for hurricane forecasting.

(ii) Our machine learning framework brings additional value to current operational models.

To validate whether a machine learning model can bring additional insights alongside current operational forecasts, we compare the accuracy of consensus models with and without our models' inclusion. In particular, we compare the impact of HURR-(stat/viz, xgb/cnn/transfo) model, as it was, in general, the most performing among all Hurricast variations which do not include forecast data as input data. We have experimented with two consensus models: simple consensus, which calculates an equal-weighted average of operational forecasts; Lasso consensus, a commonly used and straightforward regression model, that assigns different weight importance based on individual models' performance.

As shown in the bottom section of Tables A3-A6, including Hurricast model into consensus models consistently achieve higher accuracy and lower standard deviation. This effect is almost consistent throughout all testing years, for both intensity and track in both basins. This result serves as an evidence that Hurricast model can bring additional insights into the consensus models.

Compared to the NHC's Official Forecast OFCL, our consensus model including the Hurricast model can achieve higher accuracy for both basins' intensity and track forecasting. Detailed comparison can be found in Tables B7 and B8 in Appendix.

Our results highlight the complementary benefits of including a machine learning model into consensus models. As a remark, due to highly limited availability of historical operational forecast data, we believe that if given greater availability and granularity, machine learning models have still great potential to realize.

(iii) Our tree-based machine learning models can produce competitive results compared to operational statistical-numerical models on both intensity and track forecasting tasks.

Our HURR-(stat/viz, xgb/cnn/gru) and HURR-(stat/viz,

xgb/cnn/transfo) models are the most extensive and best performing variations that do not use operational forecast data. In general, they produce competitive performance with the best statistical-numerical models, outperforming almost consistently Decay-SHIPS for the intensity task, and largely outperforming CLP5 on track task. They generally underperform slightly the best numerical models. However, track forecast appears more challenging for our machine learning models and numerical models are still leading HURR variations.

Our results highlight that machine learning approaches emerge as a promising complementary approach to established methodology in the field.

(iv) Encoder-decoder standalone architectures produces competitive results with operational forecasting models.

To the best of our knowledge, our encoder-decoder architectures combining both statistical data and vision data have been applied for the first time for hurricane track forecasting and reanalysis maps feature extraction. Results suggest these architectures are competitive with the best operational statistical-numerical models for intensity forecasting. For track forecasting, the improvement over the CLP5 statistical baseline is significant but there are still limitations compared to the best operational forecasts. The GRU-decoder seems more suitable for intensity tasks while the Transformer-decoder appears better for track tasks.

8. Conclusion

This study demonstrates a novel multimodal machine learning framework for hurricane intensity and track forecasting utilizing three distinct data sources: historical storm data, reanalysis geographical maps, and operational forecasts. We present a three-step pipeline to combine multiple machine learning approaches, consisting of (1) data processing of individual data sets, (2) data fusing and feature selection, (3) prediction. We demonstrate that a successful combination of computer vision techniques and gradient-boosted trees can achieve strong predictions for both track and intensity forecasts, producing competitive results compared to current operational forecast models, especially in the intensity task.

We demonstrate that multimodal encoder-decoder architectures can successfully serve as a spatial-temporal feature extractor for downstream prediction tasks. In particular, This is also the first successful application of a Transformer-decoder architecture in hurricane forecasting.

Besides, we show that ensemble models that include our machine learning model as an input can outperform the NHC's official forecast for both intensity and track, thus demonstrating the potential value of developing machine learning approaches as a new branch methodology for hurricane forecasting.

Moreover, once trained, our models run in seconds, showing practical interest for real-time forecast, the bottleneck lying only in the reanalysis maps' acquisition.

In conclusion, our work demonstrates that machine learning can be a valuable approach to address bottlenecks in the field of TC forecasting.

Acknowledgments. We thank Louis Maestrati, Charles Guille-Escuret, Baptiste Goujaud, David Yu-Tung Hui, Sophie Giffard-Roisin, Ding Wang, Tianxing He for useful discussions. We thank Louis Maestrati, Nicolò Forcellini, Miya Wang for proof-reading. The work was partially supported from a grant to MIT by OCP Group. The authors acknowledge the MIT SuperCloud and Lincoln Laboratory Supercomputing Center for providing high performance computing resources that have contributed to the research results reported within this paper.

Data availability statement. All the data we used is open-source and can directly be accessed from the Internet with IBTrACS for hurricane features, Tropiccal for operational forecasts, ERA-5 for vision data.

APPENDIX A

Results Tables

TABLE A3. Intensity Mean Average Error (MAE) and standard deviation of the error (Error sd) of our different models, operational forecasts and consensus models on the same test set between 2017 and 2019, in the North Atlantic basin for lead time 24 h on the intensity task.

Model type	Model name	2017		2018		2019	
		Comparison on 10 TC		Comparison on 15 TC		Comparison on 12 TC	
		MAE (km)	Error sd (km)	MAE (km)	Error sd (km)	MAE (km)	Error sd (km)
Hurricast (HURR) methods	HURR-(viz, cnn/gru)	12.5	15.8	10.4	13.3	10.8	14.0
	HURR-(viz, cnn/transfo)	13.2	16.1	10.2	13.9	11.5	14.6
	HURR-(stat, xgb)	12.2	15.4	9.6	13.2	10.0	12.7
	HURR-(stat/viz, xgb/td)	12.0	14.8	9.5	13.0	9.8	12.5
	HURR-(stat/viz, xgb/cnn/gru)	11.7	14.9	9.6	12.6	10.1	13.1
	HURR-(stat/viz, xgb/cnn/transfo)	11.9	14.6	9.4	12.6	9.6	12.5
	HURR-(stat/viz/op, xgb/cnn/gru)	11.5	15.6	8.7	11.9	8.6	11.4
Operational forecasts	SHIPS	12.1	16.9	10.8	15.2	10.9	14.2
	Decay-SHIPS	10.0	13.4	10.2	13.4	10.6	13.9
	GFSO	17.3	17.8	11.2	12.9	13.5	15.5
	HWRP	10.1	12.7	8.9	12.4	9.9	12.7
	FSSE	7.7	10.9	8.9	12.2	8.7	11.4
	OFCL	8.6	11.8	8.6	12.1	8.6	11.5
Consensus models	Simple consensus op	8.5	11.3	8.4	11.5	8.5	11.2
	Simple consensus op/HURR	8.5	11.3	8.0	11.1	8.3	10.9
	Lasso Consensus op	8.0	10.2	8.2	11.5	7.9	10.6
	Lasso Consensus op/HURR	8.0	10.1	7.7	11.0	7.6	10.3

TABLE A4. Intensity Mean Average Error (MAE) and standard deviation of the error (Error sd) of our different Hurricast models, operational forecasts and consensus models on the same test set between 2016 and 2018, in the Eastern Pacific basin for lead time 24 h on the intensity task.

Eastern Pacific basin							
Model type	Model name	2016		2017		2018	
		Comparison on 15 TC		Comparison on 8 TC		Comparison on 13 TC	
		MAE (km)	Error sd (km)	MAE (km)	Error sd (km)	MAE (km)	Error sd (km)
Hurricast (HURR) methods	HURR-(viz, cnn/gru)	10.1	13.5	8.8	12.6	12.6	16.1
	HURR-(viz, cnn/transfo)	10.4	13.9	8.9	13.1	13.1	16.8
	HURR-(stat, xgb)	10.1	13.9	9.1	13.0	12.4	16.2
	HURR-(stat/viz, xgb/td)	10.2	14.0	9.1	13.2	12.6	16.3
	HURR-(stat/viz, xgb/cnn/gru)	9.6	13.2	8.9	12.6	12.0	15.6
	HURR-(stat/viz, xgb/cnn/transfo)	9.5	13.4	8.9	12.6	12.1	15.5
	HURR-(stat/viz/op, xgb/cnn/gru/transfo)	8.8	12.0	8.0	10.1	10.6	13.6
Operational forecasts	SHIPS	9.9	12.8	10.0	13.0	12.9	15.8
	Decay-SHIPS	9.7	12.6	9.5	12.7	13.0	15.9
	GFSO	13.0	16.4	11.9	16.3	19.3	20.5
	HWRP	10.4	13.7	7.9	11.6	10.9	14.9
	FSSE	8.5	11.5	7.9	10.7	9.8	12.6
	OFCL	8.7	11.9	8.1	11.7	10.2	13.5
Consensus models	Simple consensus op	8.6	11.7	7.8	10.7	10.2	13.0
	Simple consensus op/HURR	8.5	11.6	7.5	10.5	10.2	13.0
	Lasso Consensus op	8.3	11.2	7.9	10.3	8.7	12.1
	Lasso Consensus op/HURR	8.0	11.1	7.7	10.1	8.8	12.0

TABLE A5. Mean Average Error (MAE) and standard deviation of the error (Error sd) of our different models, operational forecasts and consensus models on the same test set between 2017 and 2019, in the North Atlantic basin for lead time 24 h on the tracking task.

North Atlantic basin							
Model type	Model name	2017		2018		2019	
		Comparison on 10 TC		Comparison on 15 TC		Comparison on 12 TC	
		MAE (km)	Error sd (km)	MAE (km)	Error sd (km)	MAE (km)	Error sd (km)
Hurricast (HURR) methods	HURR-(viz, cnn/gru)	94	61	113	77	123	89
	HURR-(viz, cnn/transfo)	96	57	104	56	119	83
	HURR-(stat, xgb)	132	89	143	91	142	115
	HURR-(stat/viz, xgb/td)	134	90	140	89	140	116
	HURR-(stat/viz, xgb/cnn/gru)	88	53	108	70	121	86
	HURR-(stat/viz, xgb/cnn/transfo)	94	56	102	56	117	83
Operational forecasts	CLP5	189	135	199	118	207	171
	HWRF	68	44	67	47	82	51
	GFSO	65	45	62	48	86	70
	AEMN	70	43	62	47	88	77
	FSSE	62	41	63	44	79	71
	OFCL	62	44	66	48	84	76
Consensus models	Simple consensus op	58	40	55	43	76	64
	Simple consensus op/HURR	56	38	55	39	72	61
	Lasso Consensus op	62	39	55	43	75	61
	Lasso Consensus op/HURR	57	38	55	38	71	57

TABLE A6. Mean Average Error (MAE) and standard deviation of the error (Error sd) of our different Hurricast models, operational forecasts and consensus models on the same test set between 2016 and 2018, in the Eastern Pacific basin for lead time 24 h on the tracking task.

Eastern Pacific basin							
Model type	Model name	2016		2017		2018	
		Comparison on 15 TC		Comparison on 8 TC		Comparison on 13 TC	
		MAE (km)	Error sd (km)	MAE (km)	Error sd (km)	MAE (km)	Error sd (km)
Hurricast (HURR) methods	HURR-(viz, cnn/gru)	74	40	69	42	73	45
	HURR-(viz, cnn/transfo)	74	44	67	38	76	45
	HURR-(stat, xgb)	79	46	73	41	88	50
	HURR-(stat/viz, xgb/td)	80	47	71	40	88	50
	HURR-(stat/viz, xgb/cnn/gru)	72	39	69	42	73	45
	HURR-(stat/viz, xgb/cnn/transfo)	70	43	65	38	75	44
Operational forecasts	CLP5	114	59	109	61	133	74
	HWRF	62	40	75	41	68	44
	GFSO	60	45	74	46	64	44
	AEMN	56	38	68	40	59	35
	FSSE	56	34	55	36	56	61
	OFCL	54	34	55	33	54	31
Consensus models	Simple consensus op	51	34	58	34	51	33
	Simple consensus op/HURR	48	32	54	31	47	30
	Lasso Consensus op	53	34	56	35	51	33
	Lasso Consensus op/HURR	50	33	52	28	46	30

APPENDIX B

Accuracy improvement of all models over NHC's official forecast

TABLE B7. Accuracy improvement of each Hurricast model or operational forecast compared to the NHC’s official model OFCL intensity error. Accuracy improvement is calculated as the reduction percentage in MAE error using the OFCL accuracy as a benchmark. Comparison is provided on both basins for the last 3 years of available data.

Accuracy Improvement Benchmarking to NHC Official Forecast - Intensity Forecast							
Model type	Model name	North Atlantic			East Pacific		
		2017	2018	2019	2016	2017	2018
Hurricast (HURR) methods	HURR-(viz, cnn/gru)	-45%	-21%	-26%	-16%	-9%	-24%
	HURR-(viz, cnn/transfo)	-52%	-17%	-29%	-20%	-10%	-28%
	HURR-(stat, xgb)	-42%	-12%	-16%	-16%	-12%	-22%
	HURR-(stat/viz, xgb/td)	-40%	-10%	-14%	-17%	-12%	-24%
	HURR-(stat/viz, xgb/cnn/gru)	-36%	-12%	-17%	-10%	-10%	-18%
	HURR-(stat/viz, xgb/cnn/transfo)	-38%	-9%	-12%	-9%	-11%	-19%
	HURR-(stat/viz/op, xgb/cnn/gru)	-34%	-1%	0%	-1%	1%	-4%
Operational forecasts	CLP5	-41%	-26%	-27%	-14%	-23%	-26%
	HWRP	-16%	-19%	-23%	-11%	-17%	-27%
	GFSO	-101%	-30%	-57%	-49%	-47%	-89%
	AEMN	-17%	-3%	-15%	-20%	2%	-7%
	FSSE	10%	-3%	-1%	2%	2%	4%
	OFCL	0%	0%	0%	0%	0%	0%
Consensus models	Simple consensus op	1%	2%	1%	1%	4%	0%
	Simple consensus op/HURR	1%	7%	3%	2%	7%	0%
	Lasso Consensus op	7%	5%	8%	5%	2%	15%
	Lasso Consensus op/HURR	7%	10%	12%	8%	5%	14%

TABLE B8. Accuracy improvement of each Hurricast model or operational forecast compared to the NHC’s official model OFCL track error. Accuracy improvement is calculated as the reduction percentage in MAE error using the OFCL accuracy as a benchmark. Comparison is provided on both basins for the last 3 years of available data.

Accuracy Improvement Benchmarking to NHC Official Forecast - Track Forecast							
Model type	Model name	North Atlantic			East Pacific		
		2017	2018	2019	2016	2017	2018
Hurricast (HURR) methods	HURR-(viz, cnn/gru)	-51%	-70%	-47%	-37%	-26%	-36%
	HURR-(viz, cnn/transfo)	-55%	-57%	-42%	-37%	-21%	-42%
	HURR-(stat, xgb)	-113%	-115%	-70%	-46%	-32%	-65%
	HURR-(stat/viz, xgb/td)	-116%	-112%	-67%	-48%	-29%	-64%
	HURR-(stat/viz, xgb/cnn/gru)	-42%	-63%	-45%	-33%	-24%	-36%
	HURR-(stat/viz, xgb/cnn/transfo)	-52%	-54%	-39%	-29%	-18%	-40%
	HURR-(stat/viz/op, xgb/cnn/gru/transfo)	-29%	-39%	-8%	-13%	4%	-14%
Operational forecasts	CLP5	-204%	-199%	-147%	-110%	-97%	-149%
	HWRP	-10%	0%	2%	-14%	-35%	-27%
	GFSO	-5%	7%	-2%	-12%	-33%	-19%
	AEMN	-13%	7%	-5%	-4%	-24%	-10%
	FSSE	1%	5%	6%	-3%	0%	-5%
	OFCL	0%	0%	0%	0%	0%	0%
Consensus models	Simple consensus op	6%	17%	9%	6%	-4%	5%
	Simple consensus op/HURR	10%	17%	15%	11%	3%	12%
	Lasso Consensus op	1%	17%	11%	2%	-1%	5%
	Lasso Consensus op/HURR	8%	17%	15%	7%	6%	14%

APPENDIX C

Technical components

a. Details on the CNN-encoder GRU-decoder network

We provide more formal and precise explanations of our CNN-GRU architecture.

(i) *Architecture details* Let t the instant where we want to make a 24-hour lead time prediction. Let $x_t^{\text{viz}} \in \mathbb{R}^{8 \times 9 \times 25 \times 25}$ be the corresponding spatial-temporal input of the CNN, where 8 is the number of past timesteps in the sequence, 9 is the number of pressure levels times the number of features maps, $25^\circ \times 25^\circ$ is the pixel size of each reanalysis map. Let $x_t^{\text{stat}} \in \mathbb{R}^{8 \times 31}$ be the corresponding statistical data, where 8 is the number of timesteps in the sequence, and 31 the number of features available at each timestep.

First, x_t^{viz} is embedded by the CNN into $x_t^{\text{emb}} \in \mathbb{R}^{8 \times 128}$ where 8 is the number of timesteps in the sequence, 128 is the dimension of the embedding space. Figure C6 provides an illustration of this embedding process by the CNN-encoder.

Let $i \in \{0, \dots, 7\}$ be the corresponding index of the timestep in the sequence t . At each time step t_i of the sequence, the CNN embedding $x_{t_i}^{\text{emb}}$ is concatenated with the statistical data $x_{t_i}^{\text{stat}}$ and processed as

$$h_{t_i} := \text{GRU}(h_{t_{i-1}}, [x_{t_i}^{\text{emb}}, x_{t_i}^{\text{stat}}]),$$

with $h_{t_0} = \mathbf{0}$, $h_{t_i} \in \mathbb{R}^{128}, \forall i$. $[\cdot, \cdot]$ means concatenation of the two vectors along the column axis, to keep a one-dimensional vector.

Finally, we concatenate $h_{t_0}, h_{t_1}, \dots, h_{t_7}$ to obtain a one-dimensional vector x_t^{hidden} of size $8 \cdot 128 = 1024$ and pass this vector into a series of 3 fully connected linear layers, of input-output size: (1024, 512); (512, 128); (128, c), where $c = 2$ for track forecast task and $c = 1$ for intensity task. The final layer makes the prediction.

To extract the geo-spatial embedded features, we use the output of the second fully connected layer, of dimension 128. Therefore, this technique allows to reduce $8 \cdot 9 \cdot 25 \cdot 25 = 45,000$ features into 128 predictive features, that can be input into our tree-based methods.

For each convolutional layer of the CNN, we use the following parameters: kernel size = 3, stride = 1, padding = 0. For each MaxPool layer, we use the following parameters: kernel size = 2, stride = 2, padding = 0.

The CNN-encoder architecture is largely inspired from Giffard-Roisin et al. (2020). The combination with the GRU-decoder and the feature extraction is a contribution of our work.

b. Details on the CNN-encoder Transformer-decoder network

As with the CNN-encoder GRU-decoder network, the spatial-temporal inputs are processed and concatenated

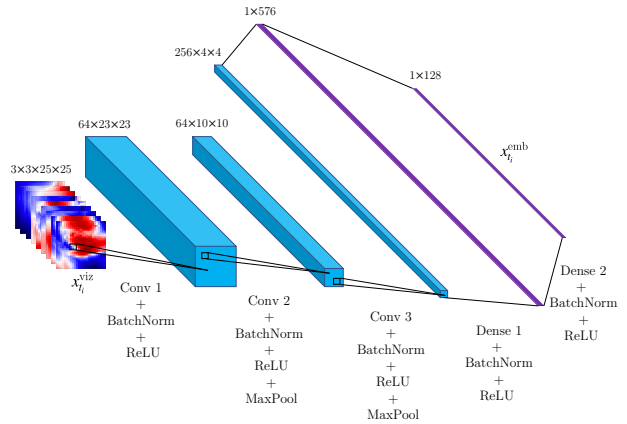


FIG. C6. Representation of our CNN-encoder. We use 3 convolutional layers, with batch normalization, ReLU and MaxPool in between. We use fully connected (dense) layers to obtain in the end a one-dimensional vector x_t^{emb} .

with the statistical data to obtain a sequence of input $[x_{t_i}^{\text{emb}}, x_{t_i}^{\text{stat}}], \forall i \in \{0, \dots, 7\}$. As suggested by Vaswani et al. (2017), we concatenate each $[x_{t_i}^{\text{emb}}, x_{t_i}^{\text{stat}}]$ input with a positional encoding P_i token in order to provide some information about the relative position i within the sequence. We eventually obtain $x = [x_{t_i}^{\text{emb}}, x_{t_i}^{\text{stat}}] + P_i$ which is being processed by the Transformer's several layers. In this work, we use $P_{i,2j} = \sin(i/10000^{2j/d})$ and $P_{i,2j+1} = \cos(i/10000^{2j/d})$, where i is the position in the sequence, j the dimension and d the dimension of the model, in our case 142. A Layer is composed of a Multi-Head attention transformation (explained below) followed by a Fully-connected layer, similar to the Transformer's encoder presented in Vaswani et al. (2017)

Following the terminology used by the authors, for $Q, K, V \in \mathbb{R}^{I_Q \times d_k}, \mathbb{R}^{I_K \times d_k}, \mathbb{R}^{I_V \times d_v}$ respectively, we define:

$$\text{Attention}(Q, K, V) = \text{softmax}\left(\frac{QK^T}{\sqrt{d_k}}\right)V$$

The Multi-Headed Attention consists in applying the attention mechanism several times:

$$\text{MultiHead}(Q, K, V) = \text{Concat}(\text{head}_1, \dots, \text{head}_h)W^O$$

where $\text{head}_i = \text{Attention}(QW_i^Q, KW_i^K, VW_i^V)$ and $W_i^Q, W_i^K, W_i^V, W_i^O$ are parameter matrices with dimensions $\mathbb{R}^{d_k/h \times d_k}, \mathbb{R}^{d_k/h \times d_k}, \mathbb{R}^{d_v/h \times d_v}, \mathbb{R}^{hd_v \times d_k}$. In this work, we use self-attention layers (i.e., $Q = K = V$), specifically 2 layers with 2 heads, the model's dimension d_k being fixed to 142 and the feedforward dimension set to 128.

The outputs of our Transformer $h_{t_0} \dots h_{t_T}$ are then averaged feature-wise to obtain the final representation of the sequence.

(i) *Loss function* The network is trained using an objective function \mathcal{L} based on a mean squared error loss on the variable of interest (maximum sustained wind speed or TC displacement) added to an $L2$ regularization term on the weights of the network:

$$\mathcal{L} := \frac{1}{N} \sum_{i=1}^N \left(y_i^{\text{true}} - y_i^{\text{pred}} \right)^2 + \lambda \sum_l \sum_{k,j} W_{k,j}^{[l]2},$$

where N is the number of predictions, y_i^{pred} the predicted forecast intensity or latitude-longitude displacements with a lead time of 24 h, y_i^{true} the ground-truth values, λ a regularization parameter chosen by validation, $W^{[l]}$ the weights of the l -th layer of the network. We minimize this loss function using the Adam optimizer.

c. Tucker decomposition for tensors

The Tucker rank decomposition of a tensor \mathcal{A} is defined as the sum of rank-1 tensors. Formally, a rank- R tensor can be expressed as:

$$\mathcal{A} = \sum_{r=1}^R s_r \mathbf{u}_{1,r} \otimes \mathbf{u}_{2,r} \cdots \otimes \mathbf{u}_{N,r}$$

where \otimes denotes the outer product of vectors. In particular, multilinear singular value decomposition (SVD), which can be understood as the higher order principle component analysis (PCA), provides algebraic techniques to calculate the decomposition of a tensor. In addition, the truncated multilinear SVD, analogous to the truncated matrix SVD, can be employed as a dimensionality reduction tool for tensors.

The multilinear SVD expresses tensor \mathcal{A} as the a small core tensor \mathcal{S} multiplied by a set of unitary matrices. The size of the core tensor, denoted by $[k_1, \dots, k_N]$, defines the Tucker rank of the tensor. Analogous to singular value decomposition (SVD) of a matrix, the entries of the core tensor $s_{i,j,k}$ correspond to the eigen-values of a matrix, and the unitary matrices $U^{(i)}$ are the corresponding eigen-vectors. Formally, the Tucker decomposition can be expressed as:

$$\mathcal{A} = \mathcal{S} \times_1 U^{(1)} \times_2 \cdots \times_N U^{(N)}$$

$$\text{where } \mathcal{A} \in \mathbb{R}^{I_1 \times I_2 \times \cdots \times I_N}$$

$$\mathcal{S} \in \mathbb{R}^{k_1 \times k_2 \times \cdots \times k_N}$$

$$U^{(i)} \in \mathbb{R}^{I_i \times k_i}$$

where each $U^{(i)}$ is a unitary matrix, i.e., its conjugate transpose is its inverse $U^{(i)*} U^{(i)} = U^{(i)} U^{(i)*} = I$, and the

mode- n product, denoted by $\mathcal{A} \times_n U$, denotes the multiplication operation of a tensor $\mathcal{A} \in \mathbb{R}^{I_1 \times I_2 \times \cdots \times I_N}$ by a matrix $U \in \mathbb{R}^{I_n \times J_n}$. It can be viewed as a slice-wise matrix product along n -th dimension. Formally:

$$(\mathcal{A} \times_n U)_{i_1 \dots j_n \dots i_N} = \sum_{i_n} a_{i_1 \dots i_n \dots i_N} u_{j_n i_n}$$

Using this notion, we can reduce the dimensionality of tensor \mathcal{A} by artificially truncating the core tensor \mathcal{S} and corresponding $U^{(i)}$. For instance, given a 4-dimensional tensor of hurricane maps, we can decide reduce the tensor to any desired rank by keeping only the desired size of core tensor \mathcal{S} . For instance, to reduce hurricane tensor data into rank $3 \times 3 \times 3 \times 3$, we first perform higher order SVD, such that \mathcal{S} reflects descending order of the singular values, and then truncate \mathcal{S} by keeping only the first $3 \times 3 \times 3 \times 3$ entries, denoted by \mathcal{S}' , and the first 3 columns of each of $U^{(i)}$, denoted by $U'^{(i)}$. Finally, a compressed tensor \mathcal{A}' can be expressed as:

$$\mathcal{A}' = \mathcal{S}' \times_1 U'^{(1)} \times_2 \cdots \times_N U'^{(N)}$$

Finally, we flatten the truncated core tensor \mathcal{S}' into a vector, which is treated as the extracted vision features in order to train tree-based model.

d. Haversine formula

Formally, the Haversine distance between one pair of predicted point and actual point, denoted by d , is calculated by:

$$d = 2R \arcsin(\sqrt{\alpha}), \text{ where}$$

$$\alpha = \sin^2\left(\frac{\hat{\phi} - \phi}{2}\right) + \cos(\hat{\phi}) \cos(\phi) \sin^2\left(\frac{\hat{\lambda} - \lambda}{2}\right)$$

where (ϕ, λ) are the actual latitude and longitude of one data point, $(\hat{\phi}, \hat{\lambda})$ are the predicted latitude and longitude, and R is Earth's radius, approximated to be the mean radius at 6,371 km.

References

- Alemay, S., J. Beltran, A. Perez, and S. Ganzfried, 2019: Predicting hurricane trajectories using a recurrent neural network. *Proceedings of the AAAI Conference on Artificial Intelligence*, Vol. 33, 468–475.
- Bahdanau, D., K. Cho, and Y. Bengio, 2014: Neural machine translation by jointly learning to align and translate. 1409.0473.
- Berrisford, P., and Coauthors, 2011: The era-interim archive version 2.0. (1), 23, URL <https://www.ecmwf.int/node/8174>.
- Bertsimas, D., and J. Dunn, 2017: Optimal classification trees. *Machine Learning*, **106** (7), 1039–1082, doi:10.1007/s10994-017-5633-9, URL <https://doi.org/10.1007/s10994-017-5633-9>.
- Bertsimas, D., J. Pauphilet, and B. V. Parys, 2019: Sparse regression: Scalable algorithms and empirical performance. 1902.06547.
- Bertsimas, D., and B. Van Parys, 2020: Sparse high-dimensional regression: Exact scalable algorithms and phase transitions. *Ann. Statist.*, **48** (1), 300–323, doi:10.1214/18-AOS1804, URL <https://doi.org/10.1214/18-AOS1804>.
- Biswas, M. K., and Coauthors, 2018: Hurricane weather research and forecasting (hwrp) model: 2018 scientific documentation. *Developmental Testbed Center*.
- Breiman, L., J. H. Friedman, R. A. Olshen, and C. J. Stone, 1984: *Classification and Regression Trees*. Wadsworth and Brooks, Monterey, CA.
- Brown, T. B., and Coauthors, 2020: Language models are few-shot learners. 2005.14165.
- Burg, T., and S. P. Lillo, 2020: Tropycal: A python package for analyzing tropical cyclones and more. *34th Conference on Hurricanes and Tropical Meteorology*, AMS.
- Carion, N., F. Massa, G. Synnaeve, N. Usunier, A. Kirillov, and S. Zagoruyko, 2020: End-to-end object detection with transformers. 2005.12872.
- Chen, R., X. Wang, W. Zhang, X. Zhu, A. Li, and C. Yang, 2019: A hybrid cnn-lstm model for typhoon formation forecasting. *Geoinformatica*, URL <https://doi.org/10.1007/s10707-019-00355-0>.
- Chen, R., W. Zhang, and X. Wang, 2020: Machine learning in tropical cyclone forecast modeling: A review. *Atmosphere*, **11** (7), 676, doi:10.3390/atmos11070676, URL <http://dx.doi.org/10.3390/atmos11070676>.
- Chen, T., and C. Guestrin, 2016: XGBoost: A scalable tree boosting system. *Proceedings of the 22nd ACM SIGKDD International Conference on Knowledge Discovery and Data Mining*, ACM, New York, NY, USA, 785–794, KDD '16, doi:10.1145/2939672.2939785, URL <http://doi.acm.org/10.1145/2939672.2939785>.
- Chen, X., Z. He, and J. Wang, 2018: Spatial-temporal traffic speed patterns discovery and incomplete data recovery via svd-combined tensor decomposition. *Transportation research part C: emerging technologies*, **86**, 59–77.
- Chung, J., Ç. Gülçehre, K. Cho, and Y. Bengio, 2014: Empirical evaluation of gated recurrent neural networks on sequence modeling. *CoRR*, **abs/1412.3555**, URL <http://arxiv.org/abs/1412.3555>.
- de Bézenac, E., A. Pajot, and P. Gallinari, 2017: Deep learning for physical processes: Incorporating prior scientific knowledge. *CoRR*, **abs/1711.07970**, URL <http://arxiv.org/abs/1711.07970>.
- De Lathauwer, L., B. De Moor, and J. Vandewalle, 2000: A multilinear singular value decomposition. *SIAM journal on Matrix Analysis and Applications*, **21** (4), 1253–1278.
- DeMaria, M., and J. Kaplan, 1994: A statistical hurricane intensity prediction scheme (ships) for the atlantic basin. *Weather and Forecasting*, **9** (2), 209–220.
- Devlin, J., M.-W. Chang, K. Lee, and K. Toutanova, 2018: Bert: Pre-training of deep bidirectional transformers for language understanding. 1810.04805.
- ECWMF, 2019: *PART III: Dynamics and Numerical Procedures*. No. 3, IFS Documentation, ECMWF, URL <https://www.ecmwf.int/node/19307>.
- ERA5, 2017: Era5 reanalysis. Research Data Archive at the National Center for Atmospheric Research, Computational and Information Systems Laboratory, Boulder CO, URL <https://doi.org/10.5065/D6X34W69>.
- Galassi, A., M. Lippi, and P. Torrioni, 2020: Attention in natural language processing. *IEEE Transactions on Neural Networks and Learning Systems*, 1–18, doi:10.1109/tnnls.2020.3019893, URL <http://dx.doi.org/10.1109/TNNLS.2020.3019893>.
- Gao, S., P. Zhao, B. Pan, Y. Li, M. Zhou, J. Xu, S. Zhong, and Z. Shi, 2018: A nowcasting model for the prediction of typhoon tracks based on a long short term memory neural network. *Acta Oceanologica Sinica*, **37**, 8–12.
- Giffard-Roisin, S., M. Yang, G. Charpiat, C. Kumler Bonfanti, B. Kégl, and C. Monteleoni, 2020: Tropical cyclone track forecasting using fused deep learning from aligned reanalysis data. *Frontiers in Big Data*, **3**, 1, doi:10.3389/fdata.2020.00001, URL <https://www.frontiersin.org/article/10.3389/fdata.2020.00001>.
- Goodfellow, I., Y. Bengio, and A. Courville, 2016: *Deep Learning*. The MIT Press.
- Grinsted, A., P. Ditlevsen, and J. H. Christensen, 2019: Normalized us hurricane damage estimates using area of total destruction, 1900–2018. *Proceedings of the National Academy of Sciences*, **116** (48), 23 942–23 946, doi:10.1073/pnas.1912277116, URL <https://www.pnas.org/content/116/48/23942>, <https://www.pnas.org/content/116/48/23942.full.pdf>.
- He, K., X. Zhang, S. Ren, and J. Sun, 2016: Deep residual learning for image recognition. *Proceedings of the IEEE conference on computer vision and pattern recognition*, 770–778.
- Hinton, G., O. Vinyals, and J. Dean, 2015: Distilling the knowledge in a neural network. 1503.02531.
- Hochreiter, S., and J. Schmidhuber, 1997: Long short-term memory. *Neural Comput.*, **9** (8), 1735–1780, doi:10.1162/neco.1997.9.8.1735, URL <https://doi.org/10.1162/neco.1997.9.8.1735>.
- Jaderberg, M., K. Simonyan, A. Zisserman, and K. Kavukcuoglu, 2015: Spatial transformer networks. *CoRR*, **abs/1506.02025**, URL <http://arxiv.org/abs/1506.02025>.
- Jarvinen, B. R., and C. J. Neumann, 1979: Statistical forecasts of tropical cyclone intensity for the north atlantic basin.
- Jetley, S., N. A. Lord, N. Lee, and P. H. S. Torr, 2018: Learn to pay attention. 1804.02391.
- Kiela, D., and L. Bottou, 2014: Learning image embeddings using convolutional neural networks for improved multi-modal semantics.

- Proceedings of the 2014 Conference on Empirical Methods in Natural Language Processing (EMNLP)*, Association for Computational Linguistics, Doha, Qatar, 36–45, doi:10.3115/v1/D14-1005, URL <https://www.aclweb.org/anthology/D14-1005>.
- Kim, S., H. Kim, J. Lee, S. Yoon, S. E. Kahou, K. Kashinath, and M. Prabhat, 2019: Deep-hurricane-tracker: Tracking and forecasting extreme climate events. *2019 IEEE Winter Conference on Applications of Computer Vision (WACV)*, 1761–1769.
- Kingma, D. P., and J. Ba, 2014: Adam: A method for stochastic optimization. URL <http://arxiv.org/abs/1412.6980>, cite arxiv:1412.6980Comment: Published as a conference paper at the 3rd International Conference for Learning Representations, San Diego, 2015.
- Knaff, J. A., M. DeMaria, C. R. Sampson, and J. M. Gross, 2003: Statistical, 5-day tropical cyclone intensity forecasts derived from climatology and persistence. *Weather and Forecasting*, **18** (1), 80–92.
- Knapp, K. R., M. C. Kruk, D. H. Levinson, H. J. Diamond, and C. J. Neumann, 2010: The international best track archive for climate stewardship (ibtracs): Unifying tropical cyclone best track data. *Bulletin of the American Meteorological Society*, 91, 363–376, URL <https://doi.org/10.1175/2009BAMS2755.1>.
- Knutson, T., and Coauthors, 2019: Tropical Cyclones and Climate Change Assessment: Part I: Detection and Attribution. *Bulletin of the American Meteorological Society*, **100** (10), 1987–2007, doi:10.1175/BAMS-D-18-0189.1, URL <https://doi.org/10.1175/BAMS-D-18-0189.1>, https://journals.ametsoc.org/bams/article-pdf/100/10/1987/4871509/bams-d-18-0189_1.pdf.
- Kolda, T. G., and B. W. Bader, 2009: Tensor decompositions and applications. *SIAM review*, **51** (3), 455–500.
- Krishnamurti, T. N., M. K. Biswas, B. P. Mackey, R. G. Ellingson, and P. H. Ruscher, 2011: Hurricane forecasts using a suite of large-scale models. *Tellus A*, **63** (4), 727–745, doi:10.1111/j.1600-0870.2011.00519.x, URL <https://onlinelibrary.wiley.com/doi/abs/10.1111/j.1600-0870.2011.00519.x>.
- Krizhevsky, A., I. Sutskever, and G. E. Hinton, 2012: Imagenet classification with deep convolutional neural networks. *Advances in neural information processing systems*, 1097–1105.
- Lan, Z., M. Chen, S. Goodman, K. Gimpel, P. Sharma, and R. Soricut, 2019: Albert: A lite bert for self-supervised learning of language representations. 1909.11942.
- Landsea, C., J. Franklin, and J. Beven, 2015: The revised atlantic hurricane database (hurdat2). *NOAA/NHC*. [Available online at nhc.noaa.gov].
- LeCun, Y., B. Boser, J. S. Denker, D. Henderson, R. E. Howard, W. Hubbard, and L. D. Jackel, 1989: Backpropagation applied to handwritten zip code recognition. *Neural computation*, **1** (4), 541–551.
- Li, S., X. Jin, Y. Xuan, X. Zhou, W. Chen, Y. Wang, and X. Yan, 2019: Enhancing the locality and breaking the memory bottleneck of transformer on time series forecasting. *CoRR*, **abs/1907.00235**, URL <http://arxiv.org/abs/1907.00235>, 1907.00235.
- Lian, J., P. Dong, Y. Zhang, J. Pan, and K. Liu, 2020: A novel data-driven tropical cyclone track prediction model based on cnn and gru with multi-dimensional feature selection. *IEEE Access*, **8**, 97 114–97 128, doi:10.1109/ACCESS.2020.2992083.
- Lian, J., P. Dong, Y. Zhang, J. Pan, and K. Liu, 2020: A novel data-driven tropical cyclone track prediction model based on cnn and gru with multi-dimensional feature selection. *IEEE Access*.
- Lin, J., K. Emanuel, and J. L. Vigh, 2020: Forecasts of Hurricanes Using Large-Ensemble Outputs. *Weather and Forecasting*, **35** (5), 1713–1731, doi:10.1175/WAF-D-19-0255.1, URL <https://doi.org/10.1175/WAF-D-19-0255.1>, <https://journals.ametsoc.org/waf/article-pdf/35/5/1713/4986082/wafd190255.pdf>.
- Liu, Y., and Coauthors, 2019: Roberta: A robustly optimized bert pretraining approach. 1907.11692.
- Moradi Kordmahalleh, M., M. Gorji Sefidmazgi, and A. Homaifar, 2016: A sparse recurrent neural network for trajectory prediction of atlantic hurricanes. *Proceedings of the Genetic and Evolutionary Computation Conference 2016*, 957–964.
- Mudigonda, M., and Coauthors, 2017: Segmenting and tracking extreme climate events using neural networks.
- Neale, R. B., and Coauthors, 2010: Description of the near community atmosphere model (cam 5.0), tech. note ncar/tn-486+str, natl. cent. for atmos. 6of7 ZHAO ET AL.: AEROSOL FIE SIMULATED BY CAMS L08806, 2009–038 451.
- Oh, J., J. Wang, and J. Wiens, 2018: Learning to exploit invariances in clinical time-series data using sequence transformer networks. *CoRR*, **abs/1808.06725**, URL <http://arxiv.org/abs/1808.06725>, 1808.06725.
- Paszke, A., and Coauthors, 2019: Pytorch: An imperative style, high-performance deep learning library. *Advances in Neural Information Processing Systems 32*, H. Wallach, H. Larochelle, A. Beygelzimer, F. d'Alché-Buc, E. Fox, and R. Garnett, Eds., Curran Associates, Inc., 8024–8035.
- Racah, E., C. Beckham, T. Maharaj, Prabhat, and C. J. Pal, 2016: Semi-supervised detection of extreme weather events in large climate datasets. *CoRR*, **abs/1612.02095**, URL <http://arxiv.org/abs/1612.02095>, 1612.02095.
- Rheme, J. R., 2007: Technical summary of the national hurricane center track and intensity models. *Updated September*, **12**, 2007.
- Rumelhart, D. E., G. E. Hinton, and R. J. Williams, 1985: Learning internal representations by error propagation. Tech. rep., California Univ San Diego La Jolla Inst for Cognitive Science.
- Shi, X., Z. Chen, H. Wang, D.-Y. Yeung, W.-k. Wong, and W.-c. Woo, 2015: Convolutional lstm network: A machine learning approach for precipitation nowcasting. *Proceedings of the 28th International Conference on Neural Information Processing Systems - Volume 1*, MIT Press, Cambridge, MA, USA, 802–810, NIPS' 15.
- Shimada, U., H. Owada, M. Yamaguchi, T. Iriguchi, M. Sawada, K. Aonashi, M. DeMaria, and K. D. Musgrave, 2018: Further Improvements to the Statistical Hurricane Intensity Prediction Scheme Using Tropical Cyclone Rainfall and Structural Features. *Weather and Forecasting*, **33** (6), 1587–1603, doi:10.1175/WAF-D-18-0021.1, URL <https://doi.org/10.1175/WAF-D-18-0021.1>, https://journals.ametsoc.org/waf/article-pdf/33/6/1587/4664604/waf-d-18-0021_1.pdf.
- Sidiropoulos, N. D., L. De Lathauwer, X. Fu, K. Huang, E. E. Papalexakis, and C. Faloutsos, 2017: Tensor decomposition for signal processing and machine learning. *IEEE Transactions on Signal Processing*, **65** (13), 3551–3582.

- Su, H., L. Wu, J. H. Jiang, R. Pai, A. Liu, A. J. Zhai, P. Tavalali, and M. DeMaria, 2020: Applying satellite observations of tropical cyclone internal structures to rapid intensification forecast with machine learning. *Geophysical Research Letters*, **47** (17), doi: 10.1029/2020GL089102, URL <https://agupubs.onlinelibrary.wiley.com/doi/abs/10.1029/2020GL089102>.
- Sønderby, C. K., and Coauthors, 2020: Metnet: A neural weather model for precipitation forecasting. 2003.12140.
- Tan, C., F. Sun, T. Kong, W. Zhang, C. Yang, and C. Liu, 2018: A survey on deep transfer learning. *CoRR*, **abs/1808.01974**, URL <http://arxiv.org/abs/1808.01974>, 1808.01974.
- Tibshirani, R., 1996: Regression shrinkage and selection via the lasso. *Journal of the Royal Statistical Society. Series B (Methodological)*, **58** (1), 267–288, URL <http://www.jstor.org/stable/2346178>.
- Van Rossum, G., and F. L. Drake Jr, 1995: *Python tutorial*. Centrum voor Wiskunde en Informatica Amsterdam, The Netherlands.
- Vaswani, A., N. Shazeer, N. Parmar, J. Uszkoreit, L. Jones, A. N. Gomez, L. u. Kaiser, and I. Polosukhin, 2017: Attention is all you need. *Advances in Neural Information Processing Systems 30*, I. Guyon, U. V. Luxburg, S. Bengio, H. Wallach, R. Fergus, S. Vishwanathan, and R. Garnett, Eds., Curran Associates, Inc., 5998–6008, URL <http://papers.nips.cc/paper/7181-attention-is-all-you-need.pdf>.
- Wang, D., B. Liu, P.-N. Tan, and L. Luo, 2020: Omulet: Online multi-lead time location prediction for hurricane trajectory forecasting. *Proceedings of the AAAI Conference on Artificial Intelligence*, **34**, 963–970, doi:10.1609/aaai.v34i01.5444.
- Wu, N., B. Green, X. Ben, and S. O’Banion, 2020: Deep transformer models for time series forecasting: The influenza prevalence case. 2001.08317.
- Yan, H., K. Paynabar, and J. Shi, 2014: Image-based process monitoring using low-rank tensor decomposition. *IEEE Transactions on Automation Science and Engineering*, **12** (1), 216–227.
- Yosinski, J., J. Clune, Y. Bengio, and H. Lipson, 2014: How transferable are features in deep neural networks? *CoRR*, **abs/1411.1792**, URL <http://arxiv.org/abs/1411.1792>, 1411.1792.
- Yun, C., S. Bhojanapalli, A. S. Rawat, S. J. Reddi, and S. Kumar, 2019: Are transformers universal approximators of sequence-to-sequence functions? 1912.10077.